Neurobiology of Disease

Chemogenetic Activation of Cortical Parvalbumin-Positive Interneurons Reverses Noise-Induced Impairments in Gap Detection

Samer Masri,[1] Nakayla Chan,[2] Tyler Marsh,[2] Alexander Zinsmaier,[2] David Schaub,[2] Li Zhang,[2] Weihua Wang,[2] and Shaowen Bao[1,2]

[1]Graduate Program in Neuroscience, University of Arizona, Tucson, Arizona 85724, and [2]Department of Physiology, University of Arizona, Tucson, Arizona 85724

Exposure to loud noises not only leads to trauma and loss of output from the ear but also alters downstream central auditory circuits. A perceptual consequence of noise-induced central auditory disruption is impairment in gap-induced prepulse inhibition, also known as gap detection. Recent studies have implicated cortical parvalbumin (PV)-positive inhibitory interneurons in gap detection and prepulse inhibition. Here, we show that exposure to loud noises specifically reduces the density of cortical PV but not somatostatin (SOM)-positive interneurons in the primary auditory cortex in mice (C57BL/6) of both sexes. Optogenetic activation of PV neurons produced less cortical inhibition in noise-exposed than sham-exposed animals, indicative of reduced PV neuron function. Activation of SOM neurons resulted in similar levels of cortical inhibition in noise- and sham-exposed groups. Furthermore, chemogenetic activation of PV neurons with the hM3-based designer receptor exclusively activated by designer drugs completely reversed the impairments in gap detection for noise-exposed animals. These results support the notions that cortical PV neurons encode gap in sound and that PV neuron dysfunction contributes to noise-induced impairment in gap detection.

Key words: **auditory processing disorder; gap detection; hearing loss; inhibition; parvalbumin; somatostatin**

Significance Statement

Noise-induced hearing loss contributes to a range of central auditory processing deficits (CAPDs). The mechanisms underlying noise-induced CAPDs are still poorly understood. Here we show that exposure to loud noises results in dysfunction of PV-positive but not somatostatin-positive inhibitory interneurons in the primary auditory cortex. In addition, cortical PV inhibitory neurons in noise-exposed animals had reduced expression of glutamic acid decarboxylases and weakened inhibition on cortical activity. Noise exposure resulted in impaired gap detection, indicative of disrupted temporal sound processing and possibly tinnitus. We found that chemogenetic activation of cortical PV inhibitory interneurons alleviated the deficits in gap detection. These results implicate PV neuron dysfunction as a mechanism for noise-induced CAPDs.

Introduction

Exposure to loud recreational and occupational noises is a major cause of hearing loss. Noise exposure can damage cochlear hair cells and the ribbon synapses of these cells onto spiral ganglionic neurons, weakening sensory input to the brain (Eggermont and Roberts, 2004; Kujawa and Liberman, 2009; Op de Beeck et al., 2011). Additionally, hearing loss can cause widespread molecular, cellular, and physiological changes in the central auditory pathway (Mühlnickel et al., 1998; Gröschel et al., 2010). Although these changes may include an increase in the excitation-to-inhibition ratio to compensate for missing thalamocortical input, they can also cause central processing disorders (Qiu et al., 2000; Seki and Eggermont, 2003; Kotak et al., 2005; Eggermont, 2006; Sun et al., 2008). One such disorder is impaired gap detection as measured with gap-induced prepulse inhibition (PPI; Aizawa and Eggermont, 2006; Turner et al., 2006). The impairment is believed to stem from pathologies in the central auditory pathway because it cannot be fully accounted for by noise-induced hearing loss (Longenecker and Galazyuk, 2011; Eggermont, 2013). For example, mice with monaural noise-induced hearing loss (NIHL) were impaired in detecting gap in sound, although they can hear the background sound as evidenced by the performance of mice in tone-induced prepulse

Received Nov. 4, 2021; revised Aug. 18, 2021; accepted Aug. 23, 2021.

Author contributions: S.M., W.W., and S.B. designed research; S.M., N.C., T.M., A.Z., D.S., L.Z., and W.W. performed research; S.M., N.C., T.M., A.Z., and W.W. analyzed data; S.M., W.W., and S.B. wrote the paper.

This work was supported in part by grants from the National Institutes of Health (DC009259) and the U.S. Department of Defense (W81XWH-15-1-0028 and W81XWH-15-1-0356).

The authors declare no competing financial interests.

Correspondence should be addressed to Weihua Wang at weihuawang@email.arizona.edu or Shaowen Bao at sbao@email.arizona.edu.

https://doi.org/10.1523/JNEUROSCI.2687-19.2021

inhibition (Wang et al., 2019). Mice deficient in tumor necrosis factor-alpha (TNF-α) gene expression exhibited normal gap detection despite monaural NIHL, indicating that monaural hearing loss alone does not impair gap detection (Wang et al., 2019).

What causes impairment in gap detection if not hearing loss itself? Studies have implicated cortical parvalbumin (PV)-positive (PV+) inhibitory interneurons in gap detection (Weible et al., 2014; Keller et al., 2018). PV neurons account for ~40% of cortical inhibitory neurons (Xu et al., 2010). They are involved in diverse functions, such as sharpening response timing, improving signal-to-noise ratio, controlling neuronal gain, and gating the critical period of developmental plasticity (Hensch and Stryker, 2004; Gabernet et al., 2005; Sohal et al., 2009; Atallah et al., 2012; Lee et al., 2012; Hamilton et al., 2013). Relevant to gap detection is recent evidence that PV neurons encode gaps in continuous background sound. Specifically, PV neurons respond more strongly than non-PV neurons to gap onset (Keller et al., 2018). Paradoxically, suppressing cortical PV neuron activity before or after the gap, which presumably weakens encoding of the gap by PV neurons, was found to enhance gap-induced prepulse inhibition (Weible et al., 2014). Furthermore, PV-deficient mice are impaired in tone-induced prepulse inhibition (Brown et al., 2015). Thus, although evidence suggests the involvement of PV neurons in gap detection, the nature of the contributions and the role of PV neurons in behavioral deficits after NIHL is unclear.

Does noise exposure alter cortical PV neuron physiology? PV neurons are modulated by sensory input. For example, deprivation of dynamic acoustic input during development can delay maturation (de Villers-Sidani et al., 2008). Depriving sound input in adulthood suppresses PV neuron function (Resnik and Polley, 2017). Previous studies also examined PV neurons following noise exposure but reported different effects; PV expression in primary auditory cortex (AI) was found to be enhanced (Liu et al., 2018) and unaltered (Nguyen et al., 2017). These discrepancies, likely because of differences in noise exposure paradigms and other procedures, make it difficult to assess the involvement of PV neurons in noise-induced impairment in gap detection.

We examined cortical PV neuron density and function following NIHL. We also looked at cortical somatostatin (SOM)-positive inhibitory neurons, another major type of inhibitory neuron that is involved in auditory processing and learning (Weible et al., 2014; Li et al., 2015; Yavorska and Wehr, 2016; Natan et al., 2017; Lakunina et al., 2020). Our monaural noise exposure paradigm resulted in significant reductions of PV neuron density and PV-neuron-mediated cortical inhibition without altering SOM neuron density or function. Furthermore, there were reductions in expression of glutamic acid decarboxylase (GAD) mRNAs and proteins in PV neurons after NIHL. Using optoelectrophysiology we demonstrate that inhibitory output by PV but not SOM neurons is significantly reduced following NIHL. Chemogenetic activation of PV neurons partially reversed noise-induced impairments in gap detection and prepulse inhibition. Our results support a role of PV neurons in gap detection and suggest that reduced PV-neuron-mediated inhibition and other changes to PV neuron physiology contribute to impairments in gap detection following NIHL.

Materials and Methods

All procedures used in this study have been approved by the University of Arizona Institutional Animal Care and Use Committee. The following strains of mice (both male and female) were used in this study: PV-Cre (B6;129P2-Pvalb$^{tm1(cre)Arbr}$/J, stock #008069, The Jackson Laboratory), SOM-Cre (Sst$^{tm2.1(cre)Zjh}$/J, stock #013044, The Jackson Laboratory) and ROSA-tdTomato (B6.Cg-Gt(ROSA)26Sor$^{tm9(CAG-tdTomato)Hze}$/J, stock #007909, The Jackson Laboratory).

NIHL and auditory brainstem response recording. Animals were anesthetized with ketamine (100 mg/kg, i.p.) and xylazine (10 mg/kg, i.p.), and maintained at 36.5°C with a homeothermic heating pad (Harvard Apparatus). Unilateral NIHL was induced by playing a continuous 8 kHz tone at 112–114 dB SPL through a custom-made piezoelectric earphone speaker to the left ear for 2 h. The right ear was protected with sound-attenuating clay. The sound level was calibrated with a Brüel and Kjær 4135 condenser microphone. Sham-exposed mice were anesthetized without undergoing NIHL.

Under ketamine/xylazine anesthesia, auditory brainstem response (ABR) tests were performed to assess hearing thresholds before and at various time points after noise exposure. ABR signals were acquired using the BioSigRP software on a TDT RX5 Sys3 recording rig. Tone pips (3 ms full-cycle sine waves of various frequencies, with 2.5 ms Cos2-gated rise/fall time, at 5 dB intensity steps from 0 to 70 dB) were delivered to a single ear through a cannulated speaker at a rate of 19 times per second. The speaker was calibrated to have <3% harmonic distortion and flat output in the entire frequency range (SigCal32, Tucker-Davis Technologies). Five hundred recordings were averaged for each frequency intensity pair. ABRs were visually examined by an experienced experimenter who was blind to the group identities of the animals. The lowest sound level that evoked discernable ABRs was determined at each testing frequency and recorded as the ABR threshold for that frequency.

Viral injections. The following viral vectors were purchased from University of North Carolina Vector Core: AAV5-EF1a-DIO-hChR2 (H134R)-EYFP-WPRE-pA (4×10^{12} viral particles/mL), AAV5-hSyn-DIO-hM3D(Gq)-mCherry (7×10^{12} viral particles/mL), and AAV5-hSyn-DIO-eGFP (4.1×10^{12} viral particles/mL). Mice received an injection in the right AI with 1 µL of an adeno-associated virus (AAV) vector through a glass micropipette (10 µL, Drummond Wiretrol) attached to a Quintessential Stereotaxic Injector (Stoelting) using procedures described previously (Hamilton et al., 2013). Briefly, a small burr hole was made over the right auditory cortex (0.7 mm in diameter, 1.75 mm rostral to λ on the temporal ridge), and virus was delivered through a small durotomy. Each injection was performed in two stages, with 0.5 µL of virus injected at a depth of 500 µm and the remaining 0.5 µL injected at 250 µm at a rate of 0.1 µL/min. Recordings were obtained after an incubation period of 14–21 d to ensure adequate expression of the viral vector throughout the auditory cortex but not to progress to cell death.

Optogenetic and chemogenetic stimulation of PV neurons. A 473 nM blue laser (model #BL473T3, Shanghai Laser and Optics Century) was used to activate channelrhodopsin-2 (ChR2)-transfected PV and SOM neurons. The laser output was calibrated using a power meter (PM100D with sensor S120C and neutral density filter NE03A-A, ThorLabs) to deliver light at an intensity of 5 mW or 160 mW/mm^2. This light intensity was chosen to be in the upper range of what is commonly seen in the literature to ensure a strong and detectable response. Laser stimulation was conducted at 3 Hz (150 ms on, 183 ms off). Photoelectric artifacts (sharp transients locked to the onset and offset of the light stimulus) were removed by excluding time points immediately surrounding the light onset (±1 ms). Mice were injected subcutaneously with clozapine-N-oxide (CNO; 1 mg/ml dissolved in isotonic saline, injected at a dose of 1 mg/kg body weight) to activate hM3D designer receptor exclusively activated by designer drugs (DREADD)-transfected PV neurons. For behavioral experiments, a gap detection or prepulse inhibition test was initiated 20 min after CNO injection. Because each behavioral testing session took ~2 h, whereas CNO activation of PV neurons only lasts ~80 min (Guettier et al., 2009), a second dose of CNO was administered 80 min after the first injection.

Electrophysiological recording. Unit responses in AI were recorded as previously described (Kim and Bao, 2009; Masri et al., 2018). AI of animals were recorded from postnatal day (P)45 to P65. Mice were anesthetized using a cocktail of ketamine (100 mg/kg) and xylazine (10 mg/kg), and placed on a homeothermic heating pad at 36.5°C (Harvard Apparatus) in a sound attenuation chamber. The head was secured with

a custom head holder that left the ears unobstructed. The right auditory cortex was exposed and kept under a layer of silicone oil to prevent desiccation. The extracellular signal was obtained using a Tucker Davis Technologies (TDT) amplifier (Medusa RA16PA), connected to TDT RX5 hardware at a sampling rate of 25 kHz using TDT software (OpenEx) running on a Windows 10 computer. Neural responses were recorded using 32-channel (4 × 8 configuration) silicon probes (NeuroNexus) over a depth of 100–800 ± 50 μm, presumably spanning the cortical layers. For multiunit spike recording, signals were bandpass filtered between 300 and 9000 Hz and thresholded at 1.5 times the SD of the signal. A TDT coupler model electrostatic speaker was used to present all acoustic stimuli into the left ear (contralateral to the recorded cortical hemisphere) in unexposed mice and the right ear in mice with NIHL. Sound and light stimulation were controlled by a TDT RZ6. Pure tone pips of 51 frequencies (4–75 kHz, 0.1 octave spacing, 5 ms cosine-squared ramps, 50 ms duration, repeated three times) at eight intensities (0–70 dB SPL, 10 dB spacing) were presented in pseudorandom order, and responses were used to reconstruct the frequency-intensity receptive field of each individual neuron. AI was identified by its tonotopic orientation—higher frequencies are represented more rostrally and slightly more dorsally. Extracellular recordings were only performed after visual confirmation of GFP or mCherry expression using a light filter, under scarring on the skull from the injection procedure. Multiunit activity was evenly sampled from AI. Single units were sorted manually using Plexon Offline Sorter. Recordings using CNO were acquired using 16-channel 4 × 4 probes and were not sorted.

Immunofluorescence staining and image analysis. Densities of PV and SOM neurons were counted as described previously (Wang et al., 2018). Briefly, mice were transcardially perfused under deep anesthesia with ice-cold PBS followed by 4% paraformaldehyde. Brains were removed and fixed in the same fixative overnight at 4°C, equilibrated in 30% sucrose, and embedded in Tissue-Tek (Sankura Finetek). Frozen coronal sections (16 μm in thickness) were collected on gelatinized glass slides. After air drying, sections were washed in PBS and penetrated with 0.1% Triton-X at room temperature for 10 min. The tissue samples were blocked with Dako serum-free blocking buffer and incubated with primary antibodies (Anti-Parvalbumin Polyclonal antibody, 1:500; catalog #PA1-933, Invitrogen) overnight at 4°C. The secondary antibodies conjugated with Alexa Fluor 488 (anti-PV antibody, Invitrogen) were incubated for 1 h at room temperature to enable fluorescent detection. After rinsing with PBS, the sections were mounted with fluorescence mounting medium (Dako) and viewed under an Olympus BX40 microscope with a digital microscope camera (C11440, Hamamatsu). Sections of AI of SOM-Cre-tdTomato mice were imaged directly. Immunofluorescent images were sampled systematically and randomly from the AI, with the experimenters blind to sample groups. All the images were taken on the same day using the same parameters. PV and SOM neurons were counted manually and normalized to the area of interest to give density.

Quantitative RT-PCR for AI tissue samples and pooled PV neurons. Ten days after noise/sham exposure, mice were deeply anesthetized with isoflurane. AI tissue was collected and stored in 100 μl RIPA buffer (150 mM sodium chloride, 1.0% Triton X-100, 0.5% sodium deoxycholate, 0.1% SDS (sodium dodecyl sulfate), 50 mM Tris, pH 8.0) at −80°C. Tissue was homogenized in RIPA buffer by sonication. The total RNA was extracted using a Quick-RNA Miniprep Kit (catalog #11328, Zymo Research). Immediately following extraction, the total RNA concentration and A260:A280 ratio of each sample was determined with NanoDrop 2000 (Thermo Scientific). A high-capacity cDNA reverse transcription kit (Thermo Fisher) was used to generate cDNA in a thermal cycler (ABI 9700, Thermo Fisher) for 2 h at 37°C. Ten nanograms of cDNA were used in each reaction of SYBR Green system (catalog #1725121, Bio-Rad Laboratories) for real-time PCR using the CFX96 real-time PCR system (Bio-Rad Laboratories). Threshold cycle (Ct) values of the target genes were normalized to the endogenous control gene (18 s). The primer sequences are listed in Table 1. In addition, we collected intracellular contents from PV neurons in AI from brain slices of PV-Cre-tdTomato mice with glass pipettes in a patch-clamp recording setup. The pipettes contained 3 μl of excitatory solution for whole-cell recording, which was prepared with RNase-free water. Care was taken to ensure that the fluorescent cytoplasm was effectively collected. Ten PV neurons were collected from each animal, and the contents of the pipette were immediately moved to 10 μl lysate buffer after collecting each neuron (Single Cell Lysis Kit, catalog #4458235, Invitrogen) with 1 uL RNase inhibitor (catalog #N8080119, Applied Biosystems). Stop solution and DNase were added into the lysate buffer according to the product instructions. The SuperScript IV First-Strand Synthesis System (catalog #18091050, Invitrogen) was used to generate cDNAs with a thermal cycler in 20 μl reaction system. A total of 4 μl of cDNA was used in each SYBR green reaction for real-time PCR. Ct values of the target genes (GAD65 and GAD67) were normalized to the Ct of the housekeeping gene ribosomal protein L13 (RPL13). RPL13 was chosen from five common housekeeping genes [RPL13 (Ribosomal Protein L13), 18S (18S Ribosomal RNA), Cyclophilin, HPRT (Hypoxanthine-guanine phosphoribosyltransferase), and GAPDH (Glyceraldehyde 3-phosphate dehydrogenase)] because of its stable expression level following our noise exposure protocol (unpublished observation). Sensitivity and linearity of the qRT-PCR measurement of the target mRNAs was confirmed with diluted samples. Differential expression between the experimental and control group was calculated using the comparative Ct method.

Table 1. Primers for RT-PCR

Primer	Sequence
PV-FW	GCAGACTCCTTCGACCACAA
PV-RV	TCAGAATGGACCCCAGCTCA
SOM-FW	ACCCCAGACTCCGTCAGTTT
SOM-RV	TACTTGGCCAGTTCCTGTTTCC
18s-FW	GTAACCCGTTGAACCCCATT
18s-RV	CCATCCAATCGGTAGTAGCG
GAD65-FW	TGCGCTCTGCTCTATGGAGA
GAD65-RV	TTCACCACGTACTGAAGCAAAA
GAD67-FW	CACAGGTCACCCTCGATTTTT
GAD67-RV	ACCATCCAACGATCTCTCTCATC
RPL13-FW	AGCCGGAATGGCATGATACTG
RPL13-RV	TATCTCACTGTAGGGCACCTC

FW, Forward primer; RV, reverse primer.

Protein preparation and Western blotting for GAD65. Ten days after noise/sham exposure, tissue from AI was collected and stored in 100 μl RIPA buffer with protease inhibitor (Sigma-Aldrich) on ice. Samples were homogenized in RIPA buffer by sonication, and centrifuged at 11,000 rpm for 30 min at 4°C to acquire the supernatant. The protein concentration was determined by Bio-Rad Protein Assay (Bio-Rad Laboratories). Fifty micrograms of each sample were separated using 12% sodium dodecyl sulfate polyacrylamide gel and transferred to a nitrocellulose membrane. Blots were blocked in 5% BSA (Sigma-Aldrich) for 2 h at room temperature. The membrane was incubated with anti-GAD65 antibody (1:1000; catalog #3988, Cell Signaling Technology) or anti-α-Tubulin antibody (1:1000; catalog #3873, Cell Signaling Technology) overnight at 4°C. After three washing steps with TBST, horseradish peroxidase-linked secondary antibody (1:5000; Santa Cruz Biotechnology) was applied for 1 h at room temperature. After washing, blots were developed on autoradiography film (Denville Scientific) using the SuperSignal West Pico chemiluminescent substrate (Thermo Fisher Scientific). Band intensity was measured with ImageJ (National Institutes of Health). Intensity data from proteins of interest were normalized to α-Tubulin internal controls and expressed as ratios.

Gap detection and prepulse inhibition. Fourteen PV-Cre mice that were transfected with the AAV5-hSyn-Dio-hM3D(Gq)-mCherry viral vector and five PV-Cre mice that were transfected with the AAV5-hSyn-DIO-eGFP viral vector underwent gap detection and prepulse inhibition tests as described previously (Wang et al., 2019) to compare performance of the mice before versus after noise exposure and with versus without CNO administration to activate PV neurons. During the testing session, a mouse was caged in a plastic container with a mesh lid. The container was placed on a piezoelectric sensor in a sound attenuation chamber. Sounds were played through an open field speaker (Fostex FT17H) fixed

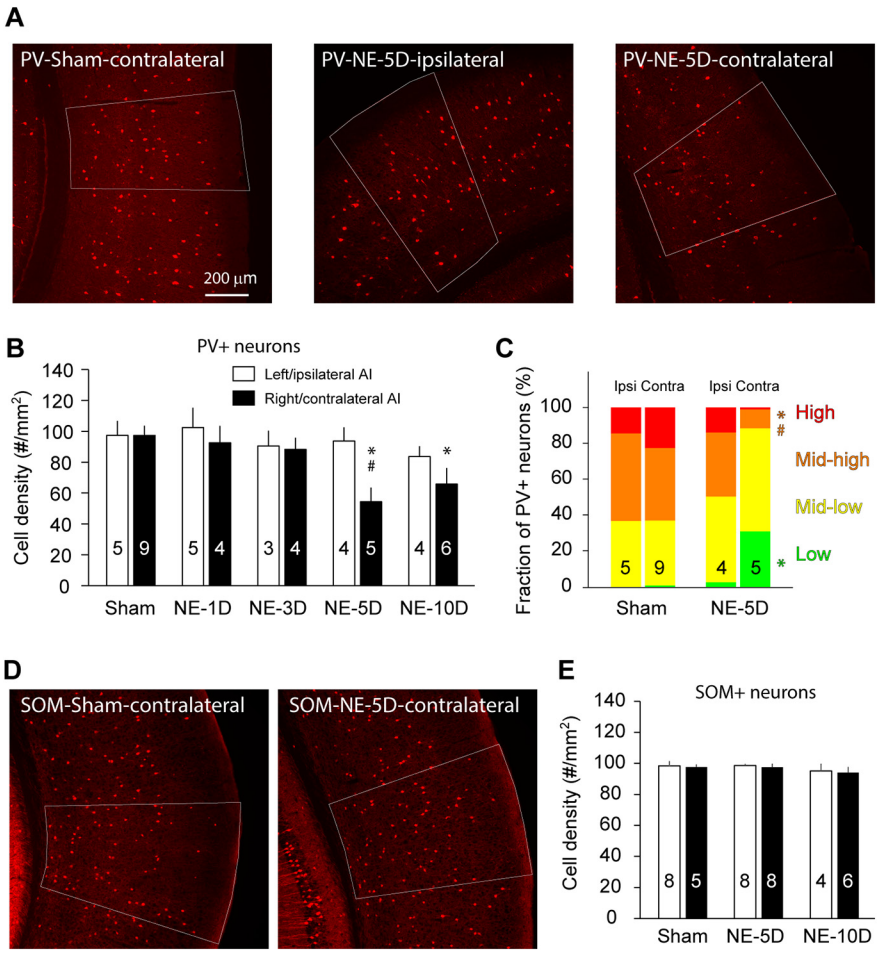

Figure 1. Noise exposure reduces the density of PV but not SOM neurons in AI. ***A***, Example images showing PV neurons in AI of sham (control)- and noise-exposed (NE) mice. ***B***, Density of PV neurons in AI of control mice, and mice 1 d, 3 d, 5 d, and 10 d after noise exposure to the left ear. ***C***, Fraction of PV+ neurons having high (>4500 a.u.), midhigh (3000–4500 a.u.), midlow (1500–3000 a.u.), and low PV (≤1500 a.u.) immunofluorescence signal levels. ***D***, Example images showing SOM neurons in AI of sham- and noise-exposed mice. ***E***, Density of SOM neurons in AI of control mice and mice 5 and 10 d after noise exposure to the left ear. Numbers of mice are indicated in the graphs as sample sizes. Data are presented as mean + SEM; *$p < 0.05$ compared with control, and #$p < 0.05$ compared with contralateral side.

above the container. The gap detection task measures the acoustic startle response elicited by a brief white noise pulse and its suppression by a preceding silent gap embedded in a continuous background sound. Each trial starts with a carrier pure tone (frequency pseudorandomly selected from 5, 7, 10, 14, 20, and 28 kHz, all at 75 dB SPL), played for a duration of 10–20 s. In uncued trials, the carrier tone was followed by a startle stimulus, a 50 ms white noise burst at 102 dB SPL. In cued trials, a 50 ms silent gap in the background sound was introduced starting 100 ms before the onset of the loud noise burst. In each testing session, the animal underwent 500 trials (50% cued and 50% uncued). After each session, we calculated the startle response ratio, which is defined as the average startle amplitude in the silent-gap-cued trials divided by the average amplitude in the uncued trials. A lower startle response ratio indicates better detection of the silent gap. A startle response ratio of one suggests that the animal failed to detect the silent gap. To assess the ability of an animal to hear a sound and perform an auditory task, animals underwent the PPI test before and after noise exposure. The test apparatus for the PPI task was identical to that of the gap detection. The test differed in that a carrier tone was absent and a white noise burst was cued by a 50 ms pure tone pulse (frequency pseudorandomly selected from 5, 7, 10, 14, 20, and 28 kHz, all at 75 dB SPL). In short, the PPI task tests the ability of an animal to detect a pure tone pulse in silence, whereas the gap detection task measures an animal's ability to detect a silent gap in a continuous pure tone.

Statistical analysis. Statistical analyses were conducted using IBM SPSS software and MATLAB. Group comparisons of variables were made using an ANOVA followed by least significant differences *post hoc*. For electrophysiological data, individual cells were used as the experimental unit for analysis. To account for sampling multiple single units from each animal, linear mixed-model tests were performed with animal identification (ID) as a random factor. The significance level was set at $\alpha = 5\%$. All data are expressed as mean ± SEM unless otherwise stated.

Results

Monaural noise exposure results in reduced PV but not SOM neuron density in contralateral AI

We first examined PV neuron density following monaural exposure to a 114 dB SPL, 8 kHz tone. This exposure paradigm has been shown to result in highly reproducible threshold shifts of up to 50 dB in the exposed ear and >10 dB on average in the protected ear (Wang et al., 2019). Auditory cortical tissues were collected 1, 3, 5, and 10 d after the noise exposure and subsequently sectioned and stained for PV (Fig. 1*A*,*B*). We observed a significant reduction in the density of PV neurons 5 and 10 d after the noise exposure compared with control, and the reduction was only observed in the contralateral side (group-by-side two-way ANOVA, group difference, $F_{(4,39)} = 3.538$, $p = 0.015$; *post hoc* tests, $p = 0.009$ for day 5 and $p = 0.010$ for day 10 after noise exposure; a hemispheric difference was observed only at 5 d after noise exposure at $p = 0.010$; Fig. 1*A*,*B*). To compare PV fluorescent signal intensity as previously described (Donato et al., 2013; Cisneros-Franco and de Villers-Sidani, 2019), we organized PV neurons into four classes based on the PV signal intensity: high [>4500 arbitrary signal unit (a.u.)], midhigh (>3000 a.u. but ≤4500 a.u.), midlow (>1500 a.u. but ≤3000 a.u.) and low (≤1500 a.u.). The reduction of PV neuron density was accompanied by a general reduction of the PV fluorescent signal intensity of PV neurons (Fig. 1*C*). The percentage of PV+ neurons with low PV signal intensities was significantly higher in the right AI of the noise-exposed group (Kruskal–Wallis test, $H_3 = 9.541$, $p = 0.023$; pairwise comparison, $p = 0.018$ for the right AI and $p = 0.264$ for the left AI), whereas the percentage of PV+ neurons with midhigh PV signal levels was significantly reduced in the right AI of the noise exposed group (Kruskal–Wallis test, $H_3 = 10.452$, $p = 0.015$; pairwise comparison, $p = 0.028$ for the right AI and $p = 0.086$ for the left AI).

We measured the density of SOM neurons 5 and 10 d after noise exposure and found no significant differences between the sham- and noise-exposed groups (group-by-side two-

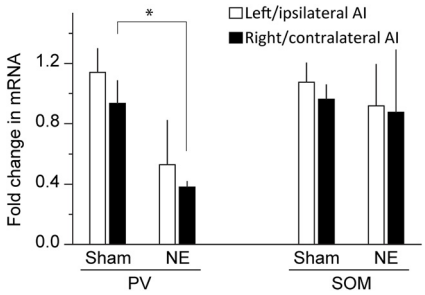

Figure 2. Noise exposure reduces PV but not SOM mRNA level in AI. PV and SOM mRNA expression levels as measured with quantitative RT-PCR. PV expression was significantly reduced in noise-exposed (NE) mice in AI in the contralateral (right) but not the ipsilateral hemisphere. By contrast, SOM expression was not significantly altered by noise exposure in AI of either hemisphere. Brain samples were collected 10 d after noise or sham exposure; $n = 4$ mice for each group; $^*p < 0.05$ versus control.

way ANOVA, group effect, $F_{(2,34)} = 0.803$, $p = 0.456$; hemispheric side, $F_{(1,34)} = 0.005$, $p = 0.942$; interaction, $F_{(2,34)} = 0.173$, $p = 0.842$, Fig. 1*D*,*E*).

Monaural noise exposure suppresses PV but not SOM mRNA levels

To complement our results from antibody staining of PV and SOM proteins (Fig. 1), we measured PV and SOM mRNA levels in AI using quantitative RT-PCR. We found that noise exposure suppressed PV expression (treatment-by-side two-way ANOVA, effect of noise exposure, $F_{(1,12)} = 20.016$, $p = 0.001$; hemispheric side, $F_{(1,12)} = 2.219$, $p = 0.162$; interaction, $F_{(1,12)} = 0.016$, $p = 0.901$, Fig. 2), but not SOM mRNA levels (treatment-by-side 2-way ANOVA, effect of noise exposure, $F_{(1,12)} = 0.252$, $p = 0.625$; hemispheric side, $F_{(1,12)} = 0.152$, $p = 0.703$; interaction, $F_{(1,12)} = 0.028$, $p = 0.870$; Fig. 2). *Post hoc* analysis indicated that PV mRNA expression levels changed significantly after NIHL in the right side ($p = 0.041$) but only had a trending difference in the left side ($p = 0.051$).

Monaural noise exposure reduces glutamate decarboxylase expression in PV neurons

Noise exposure has been shown to suppress the expression of glutamate decarboxylases (GADs) and to presynaptically weaken inhibitory synaptic transmission (Yang et al., 2011). Consistent with previous reports, we found reduced GAD65 protein levels in AI of noise-exposed mice compared with that of sham-exposed mice (treatment-by-side two-way ANOVA, effect of noise exposure, $F_{(1,17)} = 11.768$, $p = 0.003$; hemispheric side, $F_{(1,17)} = 0.682$, $p = 0.420$; interaction, $F_{(1,17)} = 2.732$, $p = 0.11$; Fig. 3*A*). A *post hoc* comparison found significant reduction of the GAD65 protein level in the right ($p < 0.05$), but not the left AI ($p > 0.05$). To determine whether GAD expression was lower specifically in PV neurons, we collected intracellular contents of PV neurons with glass pipettes from slices containing the right auditory cortex of PV-Cre-tdTomato mice. Ten PV neurons were pooled from each animal with group size of $n = 4$ mice. Quantitative RT-PCR was used to measure GAD65 and GAD67 mRNA levels. The 60S ribosomal protein L13 (RPL13) mRNA level remained constant after noise exposure (ANOVA, $F_{(1,11)} = 0.034$, $p = 0.857$, Fig. 3*B*) and was used as an internal control for sample variability. We found that both GAD65 (ANOVA, $F_{(1,10)} = 23.645$, $p = 0.001$, Fig. 3*B*) and GAD67 (ANOVA, $F_{(1,11)} = 22.052$, $p = 0.001$; Fig. 3*B*) mRNA levels were significantly reduced after noise exposure, corroborating the reduced overall GAD65 protein level in AI (Fig. 3*A*) following the same noise exposure protocol.

Monaural noise exposure attenuates PV but not SOM-neuron-mediated cortical inhibition

To determine whether reduced PV expression following noise exposure weakens the function of PV neurons, we injected viral vectors into AI of the right hemisphere of PV-Cre mice to express Cre-dependent ChR2 in auditory cortical PV neurons (Fig. 4*A*). The viral transfection marker enhanced yellow fluorescent protein (EYFP) was observed in 60.2 ± 10.5% of PV-immunoreactive neurons in AI ($n = 4$ mice). The extensive nonsomatic EYFP signal prevented reliable quantification of the percentage of viral transfected neurons that were PV immunoreactive. Four days after the viral injection, the mice underwent either noise exposure or sham exposure in the left ear. Ten days after noise exposure (14 d after the viral injection), we recorded single-unit (Fig. 4*B*) activity from AI of the right hemisphere and examined spontaneous activity during on and off epochs of laser activation of channelrhodopsin-transfected PV neurons. We isolated 220 single units from four sham-exposed mice and 115 from five noise-exposed mice. Firing rates were recorded with and without light activation of channelrhodopsin. We found that in 220 single units from the sham-exposed mice, 111 showed 50% or more suppression in spontaneous firing rate during light activation of PV neurons. In contrast, only 27 of the 115 single units of the noise-exposed group showed 50% or more suppression ($\chi^2(1) = 22.687$, $p < 0.001$; Fig. 4*C*,*D*). Binning neurons by suppression ratios reveals a rightward shift in the peak of the distribution for noise-exposed mice (Wilcoxon rank sum test, $z = 6.609$, $p < 0.001$; Fig. 4*F*).

In a separate experiment, we expressed Cre-dependent ChR2 in SOM neurons in the auditory cortex of SOM-Cre mice and examined how optogenetic activation of SOM neurons suppressed activity of cortical single units. In 168 single units recorded from two sham-exposed mice, 65 showed >50% suppression of spontaneous activity by optogenetic stimulation of SOM neurons. Similarly, 61 of the 142 single units recorded from three noise-exposed mice had >50% activity suppression ($\chi^2(1) = 0.581$, $p = 0.446$; Fig. 4*E*). The histogram of neurons binned by suppression ratios showed a nonsignificant leftward shift in the peak for noise-exposed mice, indicating a trend toward stronger SOM-neuron-mediated inhibition (Wilcoxon rank sum test, $z = 1.11$, $p = 0.267$; Fig. 4*F*). These results indicate that monaural exposure to loud noises specifically attenuates PV-neuron-mediated inhibition in AI 10 d after NIHL. To determine whether noise exposure had different effects on PV- and SOM-neuron-mediated inhibition, we performed a linear mixed-model test with neuron type (PV vs SOM) and noise exposure (exposed vs control) as fixed factors. Animal IDs were set as a random factor to account for the repeated sampling of single units from each mouse. The activity suppression ratio was used as the dependent variable. The test revealed significant effect of neuron types ($F_{(1,620.036)} = 10.869$, $p < 0.001$) and significant neuron type-by-noise exposure interaction ($F_{(1,620.601)} = 11.570$, $p < 0.001$), confirming that noise exposure differentially affected PV- and SOM-neuron-mediated cortical inhibition.

Chemogenetic activation of cortical PV neurons reverses noise-induced impairments in gap detection

The noise exposure paradigm we used in this study has been shown to result in impaired gap detection (Wang et al., 2019). To examine whether the reduction in cortical PV-neuron-mediated inhibition contributes to gap detection impairments, we tested the effects of the hM3D-activating compound CNO on behavioral performance before and after noise exposure. A group

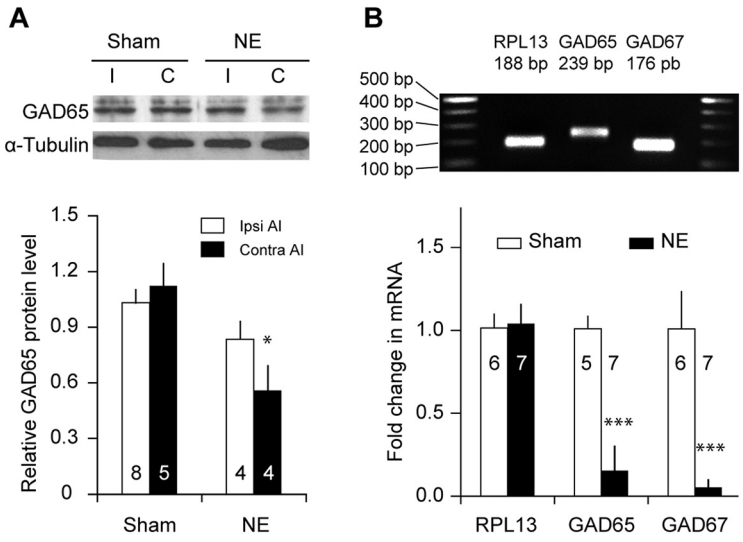

Figure 3. Noise exposure reduces GAD expression in PV neurons. ***A***, GAD65 expression was quantified with Western blot. The GAD65 protein level decreased significantly in contralateral AI after noise exposure (NE). α-Tubulin was used as an internal control. ***B***, RPL13, GAD65, and GAD67 mRNA levels were measured with qRT-PCR for samples extracted from PV neurons (see above, Materials and Methods). The mean RPL13 mRNA level was unchanged by noise exposure. GAD65 and GAD67 mRNA levels were normalized to the RPL13 mRNA level for each sample. Both GAD65 and GAD67 mRNA levels were significantly reduced in noise-exposed group; $^*p < 0.05$ compared with sham-exposed, $^{***}p < 0.005$ compared with control. Sample sizes on the graphs are numbers of mice.

of hM3D-transfected PV-Cre mice underwent four-phase behavioral tests—prenoise exposure vehicle (Pre/Veh), prenoise exposure CNO (Pre/CNO), postnoise exposure vehicle (Post/Veh) and postnoise exposure CNO (Post/CNO). Gap detection performances can be substantially variable among individual animals and different groups (Wang et al., 2019) but remain relatively stable for each animal. We therefore performed repeated-measures ANOVA and focused on within-subject effects on the four phases. For the gap detection test, a Phase × Frequency repeated-measures ANOVA revealed significant effects of the phases ($F_{(3,117)} = 3.390$, $p = 0.027$; Fig. 5*A*). Pairwise comparisons indicated that noise exposure significantly impaired gap detection (Post/Veh vs Pre/Veh, $p = 0.029$), and activation of PV neurons with CNO injection completely reversed the impairment (Post/CNO vs Pre/Veh, $p = 0.795$; Post/CNO vs Post/Veh, $p = 0.010$). Further examination indicated that the gap detection performance was different only at 20 kHz (Phase × Frequency interaction, $F_{(9,117)} = 2.544$, $p = 0.011$; $p < 0.05$ at 20 kHz, and $p > 0.05$ at 7 kHz, 10 kHz, and 14 kHz; Fig. 5*B*), which tracked performance of individual animals at 20 kHz, confirmed that noise exposure impaired gap detection (repeated-measures ANOVA, $F_{(3,39)} = 5.167$, $p = 0.004$; pairwise comparisons, Pre/Veh vs. Post/Veh, $p = 0.009$; Fig. 5*B*). Activation of PV neurons with DREADD/CNO did not alter gap detection performance before noise exposure (Pre/Veh vs Pre/CNO, $p = 0.508$) but reversed noise-induced impairment in gap detection (Pre/Veh vs Post/CNO, $p = 0.404$; Post/Veh vs Post/CNO, $p = 0.033$).

For the prepulse inhibition test, a repeated-measures ANOVA comparing the four phases across all frequencies indicated a significant effect of phases (Phase × Frequency repeated-measures ANOVA, effect of phases, $F_{(3,117)} = 5.281$, $p = 0.004$; Fig. 5*C*). However, pairwise comparison showed that activation of PV neurons with CNO injection did not affect PPI performance either before or after noise exposure ($p < 0.05$ for Pre/Veh vs Post/CNO, Pre/CNO vs Post/Veh, Pre/CNO vs Post/CNO; $p > 0.05$ for Pre/Veh vs Pre/CNO, Pre/Veh vs Post/Veh, Post/Veh vs Post/CNO).

CNO metabolizes to clozapine, which could affect behavior. To control for the potential impact of CNO metabolites on gap detection and PPI performance, we injected an AAV virus containing the GFP but not the hM3D(Gq) DREADD sequence in PV-Cre mice, and examined the performance of the animals before and after noise exposure and saline or CNO injection. We found a significant Phase × Frequency interaction in the gap detection performance (Phase × Frequency repeated-measures ANOVA, Phase × Frequency interaction, $F_{(9,63)} = 2.248$, $p = 0.030$; Fig. 5*D*). *Post hoc* analysis indicated that noise exposure significantly impaired gap detection at 20 kHz ($p = 0.038$). However, injection of CNO did not alter gap detection performance ($p = 0.905$). Furthermore, Phase × Frequency ANOVA on PPI performance indicated no significant effect of phases ($F_{(3,36)} = 1.477$, $p = 0.270$; Fig. 5*E*) or Phase × Frequency interaction ($F_{(9,36)} = 1.567$, $p = 0.163$). Our results are consistent with a previous report that CNO does not alter prepulse inhibition ratios (MacLaren et al., 2016). Together, these results indicate that activation of cortical PV neurons reverses noise-induced impairments in gap detection without altering baseline gap detection or prepulse inhibition behavior.

To confirm the efficacy and specificity of our hearing lesion paradigm we measured ABR thresholds at both ears before and 5 d after noise exposure. The hearing lesion caused a 30–40 dB increase in hearing thresholds in the exposed left ear but not the protected right ear (two-way ANOVA, Ear × NIHL interaction, $F_{(1,79)} = 137.7$, $p < 10^{-18}$; Fig. 5*F*).

We examined the efficacy of viral transfection rate in PV neurons in the hM3D-transfected PV-Cre mice. The viral transfection marker mCherry was observed in 87.8 ± 1.1% of PV-immunoreactive neurons in AI, and 80.8 ± 5.8% of mCherry-positive neurons showed PV immunoreactivity ($n = 4$ mice; Fig. 5*G*,*H*). We also performed successive extracellular multiunit recordings from one location in AI directly beneath the site of the injection 14–21 d after the virus injection and 10 d after the noise exposure or sham exposure. In sham-exposed mice ($n = 2$), administration of CNO to activate PV neurons suppressed overall spontaneous activity 65 min after the injection (one-sample t test, $t_{(31)} = 6.038$, $p < 0.001$; Fig. 5*I*). In noise-exposed mice ($n = 3$), suppression of spontaneous activity was present (one-sample t test, $t_{(80)} = 7.336$, $p < 0.001$) but significantly reduced compared with mice with intact hearing (unpaired t test, $t_{(111)} = 2.475$, $p = 0.0148$).

Discussion

There are three main findings in the present study. First, contrary to previous reports of increased and unaltered PV neuron density, we found significantly reduced PV neuron density and PV expression in AI 5 and 10 d after loud noise exposure (Nguyen et al., 2017; Liu et al., 2018). In the case of Nguyen et al. (2017), the researchers used a bilateral noise exposure paradigm with a free field speaker at a lower volume of 102–104 dB SPL which could account for our different results. In the case of Liu et al. (2018), although more similar to our paradigm, the hearing

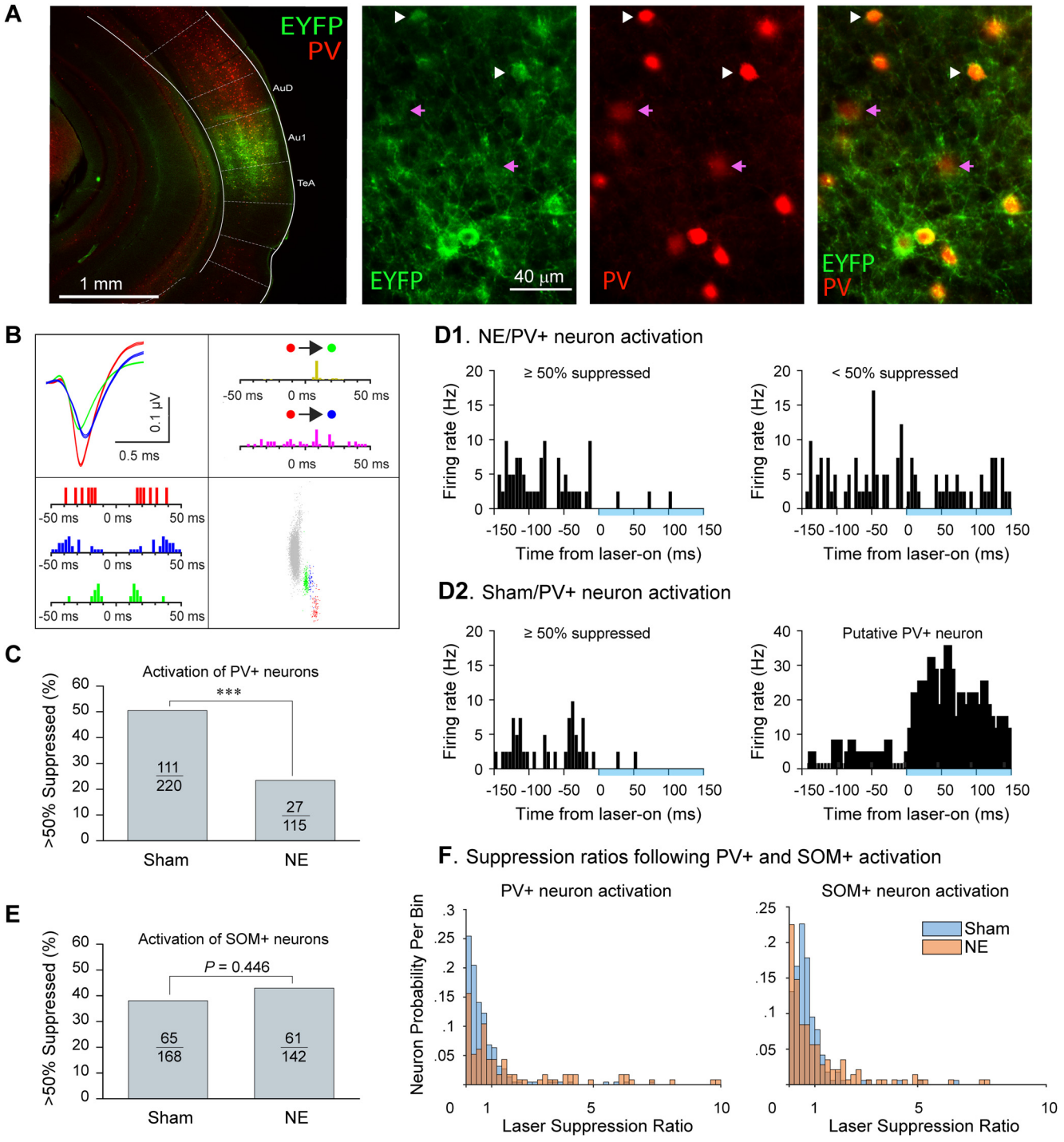

Figure 4. Cortical inhibition by PV but not SOM neurons is reduced by noise exposure. ***A***, Example images showing PV (red) and viral expression of EYFP (green) in PV neurons. Left, Low-magnification image shows viral-mediated expression of EYFP colocalized with PV in AI and nearby areas. Right, High-magnification images show PV, EYFP, and merged signals. White arrowheads point to transfected PV neurons as indicated by mCherry signal, and purple arrows point to nontransfected PV neurons. ***B***, Spike sorting example. In this case, three distinct units (red, green, and blue, MANOVA, $p < 10^{-5}$) were obtained on one channel. Top, Three distinct average waveforms (left) of sorted units ± SEM. Bottom, Autocorrelograms (left) indicate distinct activity patterns and refractory periods in the three neurons. Top, Cross-correlograms (right) indicate that the red neuron drove firing of the green neuron but not the blue neuron. Bottom, PCA analysis (right) indicates that the clusters have distinct spike waveform shapes. ***C***, Proportion of cortical single units that were strongly suppressed (>50%) by optogenetic activation of PV neurons. Noise exposure (NE) significantly reduced the proportion of strongly suppressed single units from 50 to 19%. ***D***, Example peristimulus time histograms of units that were either strongly suppressed or not strongly suppressed by optogenetic activation of PV neurons from both sham- and noise-exposed populations. Blue bars indicate laser onset time. Bottom, Peristimulus time histogram shows a laser-activated putative PV neuron (right). ***E***, Proportion of cortical single units that were strongly suppressed by optogenetic activation of SOM neurons. ***F***, Histograms showing the distributions of laser on/laser off suppression ratios among isolated neurons from sham- and noise-exposed mice of both PV:Cre and SOM:Cre lines. Histograms are normalized to an area of one. A ratio less than one indicates that laser activation of either PV or SOM neurons inhibited spiking; ***$p < 0.001$. Sample sizes on the graphs are numbers of single units.

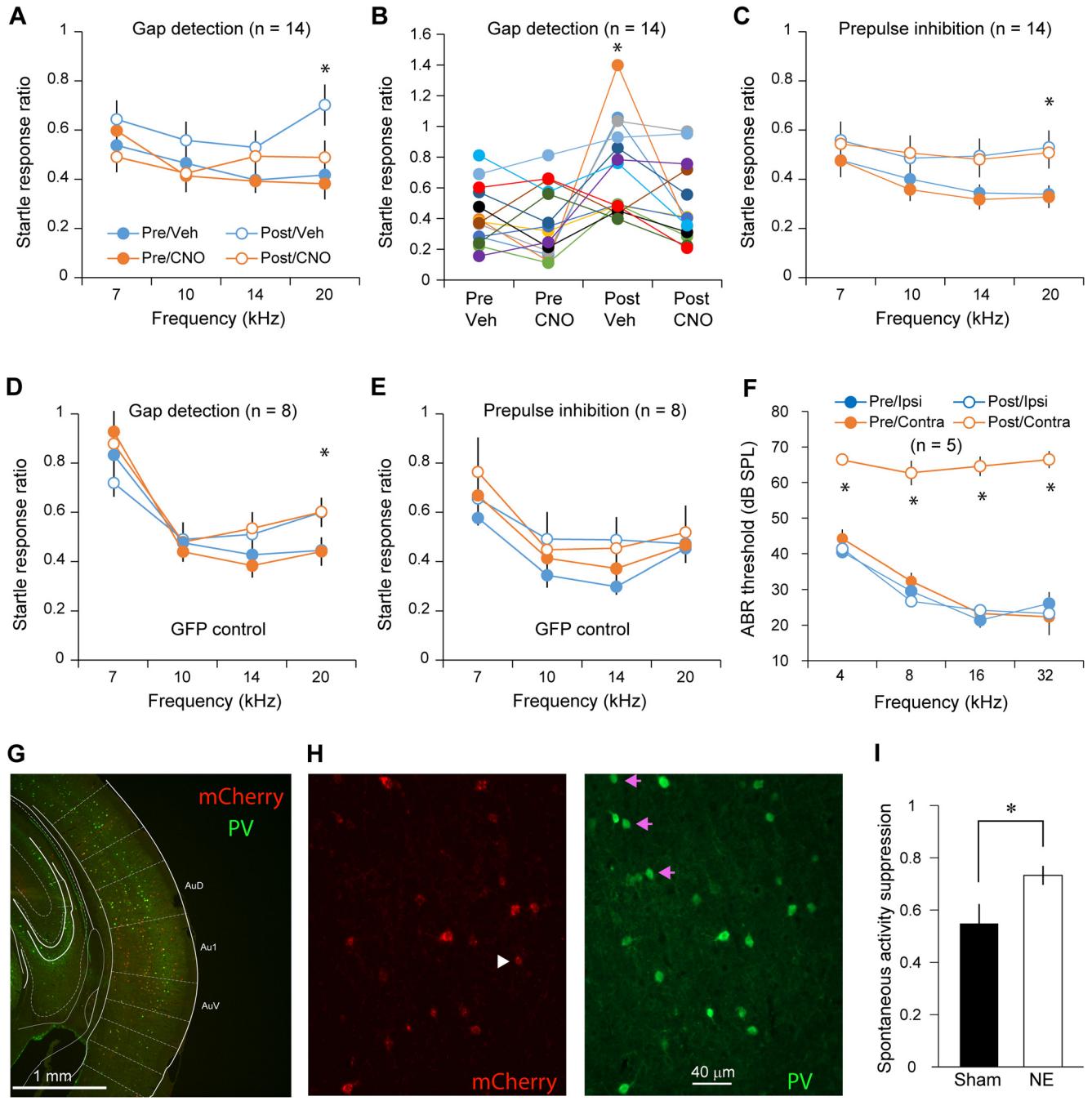

Figure 5. Chemogenetic activation of PV neurons reversed impairments in gap detection in noise-exposed animals. ***A***, Noise exposure significantly impaired gap detection performance. CNO injection in mice with hM3D expression in PV neurons completely reversed the impairments in gap detection after hearing lesions but did not change behavior before hearing lesions. ***B***, Gap detection performance from individual mice at 20 kHz. ***C***, Noise exposure reduces the effect of prepulse inhibition on the startle response ratio. CNO injection did not have an impact on behavior. All mice were tested before and after CNO injections. ***D***, CNO did not alter gap detection performance in mice with GFP expression in PV neurons. ***E***, CNO did not alter PPI performance in mice with GFP expression in PV neurons. ***F***, ABR thresholds were significantly greater only in the left ear 10 d after hearing lesions; * indicates a statistically significant difference for the frequency bin and between the treatment conditions. Sample sizes on the graphs are numbers of mice. ***G***, Example image showing the extent of Cre-dependent expression of hM3D as indicated by the mCherry reporter expression. ***H***, Example images showing colocalization of mCherry and PV immunolabeling signal in AI neurons. The white arrowhead and pink arrows point to mCherry-only and PV-only cells, respectively. ***I***, Ratio of multiunit spontaneous activity 5 min before and 65 min after CNO injection to activate PV neurons in sham-exposed ($n = 32$ multiunits/2 mice) and noise-exposed ($n = 81$ multiunits/3 mice) mice. Noise exposure significantly reduced the inhibitory effect of CNO; *$p < 0.05$.

lesion was conducted at a higher frequency of 16 kHz (in rats, which have a lower hearing range), and only for 1 h rather than two. Our result is consistent with findings that NIHL reduced cortical inhibitory synaptic transmission and PV neuron function after noise exposure (Qiu et al., 2000; Seki and Eggermont, 2003; Kotak et al., 2005; Eggermont, 2006; Sun et al., 2008; Yang et al., 2011; Wang et al., 2019). We further extended those findings by showing that the reduction is specific to PV but not SOM neurons and specific to the hemisphere contralateral to the exposed ear. We also found that noise exposure caused a reduction of PV mRNA levels but not SOM mRNA levels, corroborating the cell count results.

Second, we found that NIHL significantly reduces the inhibitory effect of optogenetic activation of the PV neuron

population. This is consistent with a previous report using drug-induced hearing loss (Resnik and Polley, 2017). Activation of SOM neurons produced similar levels of cortical inhibition in noise- and sham-exposed groups. These results are consistent with our findings of reduced PV but not SOM neuron density in the auditory cortex. Additionally, overall levels of inhibition induced by our optogenetic stimulus in both PV-Cre and Som-Cre sham-exposed mice are in general agreement with past literature (Lee et al., 2014). Our optogenetic recordings were guided by and conducted in a region of GFP fluorescence visualized through a GFP filter. However, the GFP expression levels could not be analyzed on an animal-by-animal basis as the acute recording-related damage prevented further histologic analysis. Therefore, it remains possible, although statistically unlikely, that variability in viral expression levels may alter experimental conclusions. Using a chemogenetic approach, we also observed a similar reduction in PV-neuron-mediated inhibition of spontaneous activity in noise-exposed mice.

Third, we showed that activation of PV neurons in the contralateral AI using DREADD reversed noise-induced impairments in gap detection. We confirmed that this manipulation leads to an expected reduction in spontaneous firing in AI. This finding lends support to the notion that cortical fast-spiking neurons, such as PV neurons, represent gaps in continuous sounds (Keller et al., 2018). It is also possible that the noise-induced impairment in gap detection was because of the reduction of cortical inhibition, and increasing cortical inhibition by activating any inhibitory neurons can ameliorate the impairment. Nevertheless, our results point to the reduction of cortical inhibition, presumably as a result of PV neuron dysfunction, as an important contributor to noise-induced central auditory processing disorder.

PV neurons are implicated in diverse cortical functions, which could be disrupted by exposure to loud noises and/or the subsequent loss of thalamocortical input (Hensch and Stryker, 2004; Gabernet et al., 2005; Sohal et al., 2009; Atallah et al., 2012; Lee et al., 2012; Hamilton et al., 2013). For example, noise exposure is a risk factor for tinnitus, hyperacusis, and other central auditory processing disorders (Schmuzigert et al., 2006; Hope et al., 2013; Guest et al., 2017). PV neuron dysfunction may play a role in those pathologies. These data do not allow us to differentiate between the death of PV neurons and reduction of PV expression as the mechanism of the apparent PV cell loss. However, previous publications indicate PV expression is modulated by activity (Donato et al., 2013; Dehorter et al., 2015). Our cell type-specific rtPCR experiments suggest that reduced expression of PV, GAD65, and GAD67 genes contributed to the observed reduction of PV neuron density and PV neuron function.

Our results indicate that inhibitory output from PV neurons is reduced after hearing loss and that chemogenetically activating these neurons can ameliorate related behavioral deficits in gap detection. The reduction in PV-neuron-mediated inhibition we observed may elevate neuronal excitability, resulting in tinnitus and hyperacusis (Llano et al., 2012; Yang and Bao, 2013; Auerbach et al., 2014; Ferguson and Gao, 2018). Disruptions to the function of PV neurons in sharpening response timing to dynamic stimuli, improving feature selectivity, and enhancing signal-to-noise ratio may contribute to central auditory processing disorder (Wehr and Zador, 2003; Gabernet et al., 2005; Sohal et al., 2009; Atallah et al., 2012; Lee et al., 2012; 2014; Keller et al., 2018). Furthermore, activation of PV neurons has been shown to enhance feedforward functional connectivity and information flow from the thalamus to layer 2/3 of the cortex (Hamilton et al., 2013). PV neuron dysfunction may thus impair gap detection by interrupting this information flow in the thalamocortical circuit. Gap detection is impaired in humans and animal models with tinnitus and central auditory processing disorder and is used to test for tinnitus and temporal sound processing (Turner et al., 2006; Yang et al., 2007; Suta et al., 2008; Dias et al., 2012; Fournier and Hébert, 2013; Mehdizade Gilani et al., 2013). The rescue of noise-induced impairments in gap detection by chemogenetic activation of PV neurons supports a role of PV neuron dysfunction in tinnitus and central auditory processing disorder and points to possible therapeutic targets.

References

Aizawa N, Eggermont JJ (2006) Effects of noise-induced hearing loss at young age on voice onset time and gap-in-noise representations in adult cat primary auditory cortex. J Assoc Res Otolaryngol 7:71–81.

Atallah BV, Bruns W, Carandini M, Scanziani M (2012) Parvalbumin-expressing interneurons linearly transform cortical responses to visual stimuli. Neuron 73:159–170.

Auerbach BD, Rodrigues PV, Salvi RJ (2014) Central gain control in tinnitus and hyperacusis. Front Neurol 5:206.

Brown JA, Ramikie TS, Schmidt MJ, Báldi R, Garbett K, Everheart MG, Warren LE, Gellért L, Horváth S, Patel S, Mirnics K (2015) Inhibition of parvalbumin-expressing interneurons results in complex behavioral changes. Mol Psychiatry 20:1499–1507.

Cisneros-Franco JM, de Villers-Sidani É (2019) Reactivation of critical period plasticity in adult auditory cortex through chemogenetic silencing of parvalbumin-positive interneurons. Proc Natl Acad Sci U S A 116:26329–26331.

Dehorter N, Ciceri G, Bartolini G, Lim L, del Pino I, Marín O (2015) Tuning of fast-spiking interneuron properties by an activity-dependent transcriptional switch. Science 349:1216–1220.

de Villers-Sidani E, Simpson KL, Lu YF, Lin RC, Merzenich MM (2008) Manipulating critical period closure across different sectors of the primary auditory cortex. Nat Neurosci 11:957–965.

Dias KZ, Jutras B, Acrani IO, Pereira LD (2012) Random Gap Detection Test (RGDT) performance of individuals with central auditory processing disorders from 5 to 25 years of age. Int J Pediatr Otorhinolaryngol 76:174–178.

Donato F, Rompani SB, Caroni P (2013) Parvalbumin-expressing basket-cell network plasticity induced by experience regulates adult learning. Nature 504:272–276.

Eggermont J (2006) Cortical tonotopic map reorganization and its implications for treatment of tinnitus. Acta Otolaryngol Suppl 126:9–12.

Eggermont JJ (2013) Hearing loss, hyperacusis, or tinnitus: what is modeled in animal research? Hear Res 295:140–149.

Eggermont JJ, Roberts LE (2004) The neuroscience of tinnitus. Trends Neurosci 27:676–682.

Ferguson BR, Gao WJ (2018) PV Interneurons: critical regulators of E/I balance for prefrontal cortex-dependent behavior and psychiatric disorders. Front Neural Circuits 12:37.

Fournier P, Hébert S (2013) Gap detection deficits in humans with tinnitus as assessed with the acoustic startle paradigm: does tinnitus fill in the gap? Hear Res 295:16–23.

Gabernet L, Jadhav SP, Feldman DE, Carandini M, Scanziani M (2005) Somatosensory integration controlled by dynamic thalamocortical feed-forward inhibition. Neuron 48:315–327.

Gröschel M, Götze R, Ernst A, Basta D (2010) Differential impact of temporary and permanent noise-induced hearing loss on neuronal cell density in the mouse central auditory pathway. J Neurotrauma 27:1499–1507.

Guest H, Munro KJ, Prendergast G, Howe S, Plack CJ (2017) Tinnitus with a normal audiogram: relation to noise exposure but no evidence for cochlear synaptopathy. Hear Res 344:265–274.

Guettier JM, Gautam D, Scarselli M, Ruiz de Azua I, Li JH, Rosemond E, Ma X, Gonzalez FJ, Armbruster BN, Lu H, Roth BL, Wess J (2009) A chemical-genetic approach to study G protein regulation of beta cell function in vivo. Proc Natl Acad Sci U S A 106:19197–19202.

Hamilton LS, Sohl-Dickstein J, Huth AG, Carels VM, Deisseroth K, Bao S (2013) Optogenetic activation of an inhibitory network enhances feedforward functional connectivity in auditory cortex. Neuron 80:1066–1076.

Hensch TK, Stryker MP (2004) Columnar architecture sculpted by GABA circuits in developing cat visual cortex. Science 303:1678–1681.

Hope AJ, Luxon LM, Bamiou DE (2013) Effects of chronic noise exposure on speech-in-noise perception in the presence of normal audiometry. J Laryngol Otol 127:233–238.

Keller CH, Kaylegian K, Wehr M (2018) Gap encoding by parvalbumin-expressing interneurons in auditory cortex. J Neurophysiol 120:105–114.

Kim H, Bao S (2009) Selective increase in representations of sounds repeated at an ethological rate. J Neurosci 29:5163–5169.

Kotak VC, Fujisawa S, Lee FA, Karthikeyan O, Aoki C, Sanes DH (2005) Hearing loss raises excitability in the auditory cortex. J Neurosci 25:3908–3918.

Kujawa SG, Liberman MC (2009) Adding insult to injury: cochlear nerve degeneration after "temporary" noise-induced hearing loss. J Neurosci 29:14077–14085.

Lakunina AA, Nardoci MB, Ahmadian Y, Jaramillo S (2020) Somatostatin-expressing interneurons in the auditory cortex mediate sustained suppression by spectral surround. J Neurosci 40:3564–3575.

Lee S-H, Kwan AC, Zhang S, Phoumthipphavong V, Flannery JG, Masmanidis SC, Taniguchi H, Huang ZJ, Zhang F, Boyden ES, Deisseroth K, Dan Y (2012) Activation of specific interneurons improves V1 feature selectivity and visual perception. Nature 488:379–383.

Lee S-H, Kwan AC, Dan Y (2014) Interneuron subtypes and orientation tuning. Nature 508:E1–E2.

Li LY, Xiong XR, Ibrahim LA, Yuan W, Tao HW, Zhang LI (2015) Differential receptive field properties of parvalbumin and somatostatin inhibitory neurons in mouse auditory cortex. Cereb Cortex 25:1782–1791.

Liu C, Xu T, Liu X, Huang Y, Wang H, Luo B, Sun J (2018) Acoustic trauma changes the parvalbumin-positive neurons in rat auditory cortex. Neural Plast 2018:9828070.

Llano DA, Turner J, Caspary DM (2012) Diminished cortical inhibition in an aging mouse model of chronic tinnitus. J Neurosci 32:16141–16148.

Longenecker RJ, Galazyuk AV (2011) Development of tinnitus in CBA/CaJ mice following sound exposure. J Assoc Res Otolaryngol 12:647–658.

MacLaren DA, Browne RW, Shaw JK, Radhakrishnan SK, Khare P, España RA, Clark SD (2016) Clozapine N-oxide administration produces behavioral effects in Long–Evans rats: implications for designing DREADD experiments. eNeuro 3:ENEURO.0219–16.2016.

Masri S, Zhang LS, Luo H, Pace E, Zhang J, Bao S (2018) Blast exposure disrupts the tonotopic frequency map in the primary auditory cortex. Neuroscience 379:428–434.

Mehdizade Gilani V, Ruzbahani M, Mahdi P, Amali A, Nilforush Khoshk MH, Sameni J, Karimi Yazdi A, Emami H (2013) Temporal processing evaluation in tinnitus patients: results on analysis of gap in noise and duration pattern test. Iran J Otorhinolaryngol 25:221–226.

Mühlnickel W, Elbert T, Taub E, Flor H (1998) Reorganization of auditory cortex in tinnitus. Proc Natl Acad Sci U S A 95:10340–10343.

Natan RG, Rao W, Geffen MN (2017) Cortical interneurons differentially shape frequency tuning following adaptation. Cell Rep 21:878–890.

Nguyen A, Khaleel HM, Razak KA (2017) Effects of noise-induced hearing loss on parvalbumin and perineuronal net expression in the mouse primary auditory cortex. Hear Res 350:82–90.

Op de Beeck K, Schacht J, Van Camp G (2011) Apoptosis in acquired and genetic hearing impairment: the programmed death of the hair cell. Hear Res 281:18–27.

Qiu C, Salvi R, Ding D, Burkard R (2000) Inner hair cell loss leads to enhanced response amplitudes in auditory cortex of unanesthetized chinchillas: evidence for increased system gain. Hear Res 139:153–171.

Resnik J, Polley DB (2017) Fast-spiking GABA circuit dynamics in the auditory cortex predict recovery of sensory processing following peripheral nerve damage. Elife 6:e21452.

Schmuzigert N, Fostiropoulos K, Probst R (2006) Long-term assessment of auditory changes resulting from a single noise exposure associated with non-occupational activities. Int J Audiol 45:46–54.

Seki S, Eggermont JJ (2003) Changes in spontaneous firing rate and neural synchrony in cat primary auditory cortex after localized tone-induced hearing loss. Hear Res 180:28–38.

Sohal VS, Zhang F, Yizhar O, Deisseroth K (2009) Parvalbumin neurons and gamma rhythms enhance cortical circuit performance. Nature 459:698–702.

Sun W, Zhang L, Lu J, Yang G, Laundrie E, Salvi R (2008) Noise exposure-induced enhancement of auditory cortex response and changes in gene expression. Neuroscience 156:374–380.

Suta D, Popelar J, Syka J (2008) Coding of communication calls in the subcortical and cortical structures of the auditory system. Physiol Res 57 Suppl 3:S149–159.

Turner JG, Brozoski TJ, Bauer CA, Parrish JL, Myers K, Hughes LF, Caspary DM (2006) Gap detection deficits in rats with tinnitus: a potential novel screening tool. Behav Neurosci 120:188–195.

Wang W, Zinsmaier AK, Firestone E, Lin R, Yatskievych TA, Yang S, Zhang J, Bao S (2018) Blocking tumor necrosis factor-alpha expression prevents blast-induced excitatory/inhibitory synaptic imbalance and parvalbumin-positive interneuron loss in the hippocampus. J Neurotrauma 35:2306–2316.

Wang W, Zhang LS, Zinsmaier AK, Patterson G, Leptich EJ, Shoemaker SL, Yatskievych TA, Gibboni R, Pace E, Luo H, Zhang J, Yang S, Bao S (2019) Neuroinflammation mediates noise-induced synaptic imbalance and tinnitus in rodent models. PLoS Biol 17:e3000307.

Wehr M, Zador AM (2003) Balanced inhibition underlies tuning and sharpens spike timing in auditory cortex. Nature 426:442–446.

Weible AP, Moore AK, Liu C, DeBlander L, Wu H, Kentros C, Wehr M (2014) Perceptual gap detection is mediated by gap termination responses in auditory cortex. Curr Biol 24:1447–1455.

Xu X, Roby KD, Callaway EM (2010) Immunochemical characterization of inhibitory mouse cortical neurons: three chemically distinct classes of inhibitory cells. J Comp Neurol 518:389–404.

Yang G, Lobarinas E, Zhang L, Turner J, Stolzberg D, Salvi R, Sun W (2007) Salicylate induced tinnitus: behavioral measures and neural activity in auditory cortex of awake rats. Hear Res 226:244–253.

Yang S, Bao S (2013) Homeostatic mechanisms and treatment of tinnitus. Restor Neurol Neurosci 31:99–108.

Yang S, Weiner BD, Zhang LS, Cho SJ, Bao S (2011) Homeostatic plasticity drives tinnitus perception in an animal model. Proc Natl Acad Sci U S A 108:14974–14979.

Yavorska I, Wehr M (2016) Somatostatin-expressing inhibitory interneurons in cortical circuits. Front Neural Circuits 10:76.